

# Accurate Mass Determinations in Decay Chains with Missing Energy

Hsin-Chia Cheng<sup>a</sup>, Dalit Engelhardt<sup>b</sup>, John F. Gunion<sup>a</sup>, Zhenyu Han<sup>a</sup>, and Bob McElrath<sup>c</sup>

<sup>a</sup>Department of Physics, University of California, Davis, CA 95616,

<sup>b</sup>Department of Physics, Boston University, Boston, MA 02215, <sup>c</sup>CERN, Geneva 23, Switzerland

Many beyond the Standard Model theories include a stable dark matter candidate that yields missing / invisible energy in collider detectors. If observed at the Large Hadron Collider, we must determine if its mass and other properties (and those of its partners) predict the correct dark matter relic density. We give a new procedure for determining its mass with small error.

One of the most dramatic possibilities for the Large Hadron Collider (LHC) is observation of events with large missing energy compatible with the production of a stable, weakly-interacting particle that could explain the universe's relic dark matter content. Many beyond the Standard Model (SM) theories contain such a particle, denoted  $N$ . In particular, in the Minimal Supersymmetric Standard Model (MSSM) the lightest neutralino  $\tilde{\chi}_1^0$  is stable if  $R$ -parity is conserved. Each LHC event must contain two  $N$ 's that each emerge at the end of a chain decay. For example, in the MSSM, a large production rate is associated with squark pair,  $\tilde{q}\tilde{q}$ , production, and each  $\tilde{q}$  can have substantial probability to decay via  $\tilde{q} \rightarrow q\tilde{\chi}_2^0 \rightarrow q\tilde{\ell}\ell \rightarrow q\tilde{\ell}\tilde{\chi}_1^0$  ( $\ell = e, \mu, \tau$ ), where  $\tilde{\chi}_2^0$  and  $\tilde{\ell}$  are the 2nd lightest neutralino and slepton, respectively. More generally, we will use the notation  $Z \rightarrow 7+Y \rightarrow 7+5+X \rightarrow 7+5+3+1(=N)$ , where particles 7, 5 and 3 are Standard Model jets or leptons and  $Z$ ,  $Y$ , and  $X$  are the intermediate on-shell resonances of the model in question. This event structure is illustrated in Fig. 1. This letter gives a procedure for accurately determining  $M_Z$ ,  $M_Y$ ,  $M_X$  and  $M_N$  for this topology.

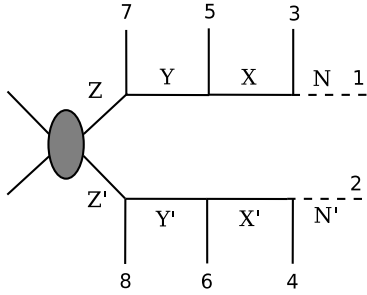


FIG. 1: The event topology.

Many mass determination procedures in the literature examine only one decay chain at a time [1, 2, 3, 4]. This often does not allow one to solve for the event's missing momenta. An exception is a very long decay chain starting from the gluino, as discussed in Ref. [2]. However, in the actual analysis the  $\tilde{\chi}_2^0$ ,  $\tilde{\ell}$  and  $\tilde{\chi}_1^0$  masses were assumed to be known and only the gluino and sbottom masses were fitted [5]. Considering both decay chains simultaneously can potentially give us more information and allow a better determination of the masses [6, 7, 8]. Our current procedure does this for the decay chains of

Fig. 1. If all particles can be correctly located on the decay chains and there are no experimental effects, then by considering two events we can solve for *all* the 4-momenta in both events and determine all the masses up to a discrete ambiguity. After examining a small number of event pairings, a unique solution will emerge.

Assuming we can isolate LHC events with the topology in Fig. 1 and using  $m_N = m_{N'}$ ,  $m_X = m_{X'}$ ,  $m_Y = m_{Y'}$ ,  $m_Z = m_{Z'}$ , we have the following constraints,

$$\begin{aligned} (M_Z^2) &= (p_1 + p_3 + p_5 + p_7)^2 = (p_2 + p_4 + p_6 + p_8)^2, \\ (M_Y^2) &= (p_1 + p_3 + p_5)^2 = (p_2 + p_4 + p_6)^2, \\ (M_X^2) &= (p_1 + p_3)^2 = (p_2 + p_4)^2, \\ (M_N^2) &= p_1^2 = p_2^2. \end{aligned} \quad (1)$$

where  $p_i$  is the 4-momentum for particle  $i$  ( $i = 1 \dots 8$ ). Since the only invisible particles are 1 and 2 and since we can measure the missing transverse energy, there are two more constraints:

$$p_1^x + p_2^x = p_{miss}^x, \quad p_1^y + p_2^y = p_{miss}^y. \quad (2)$$

Given the 6 constraints in Eqs. (1) and (2) and 8 unknowns from the 4-momenta of the missing particles, there remain two unknowns per event. The system is under-constrained and cannot be solved. This situation changes if we use a second event with the same decay chains, under the assumption that the invariant masses are the same in the two events. Denoting the 4-momenta in the second event as  $q_i$  ( $i = 1 \dots 8$ ), we have 8 more unknowns,  $q_1$  and  $q_2$ , but 10 more equations,

$$\begin{aligned} q_1^2 &= q_2^2 = p_2^2, \\ (q_1 + q_3)^2 &= (q_2 + q_4)^2 = (p_2 + p_4)^2, \\ (q_1 + q_3 + q_5)^2 &= (q_2 + q_4 + q_6)^2 = (p_2 + p_4 + p_6)^2, \\ (q_1 + q_3 + q_5 + q_7)^2 &= (q_2 + q_4 + q_6 + q_8)^2 \\ &= (p_2 + p_4 + p_6 + p_8)^2, \\ q_1^x + q_2^x &= q_{miss}^x, \quad q_1^y + q_2^y = q_{miss}^y. \end{aligned} \quad (3)$$

Altogether, we have 16 unknowns and 16 equations. The system can be solved numerically and we obtain discrete solutions for  $p_1$ ,  $p_2$ ,  $q_1$ ,  $q_2$  and thus the masses  $m_N$ ,  $m_X$ ,  $m_Y$ , and  $m_Z$ . Note that the equations always have 8 complex solutions, but we will keep only the real and positive ones which we henceforth call "solutions". Further details regarding practical and high-speed techniques for obtaining the solutions will appear in a future paper [9].

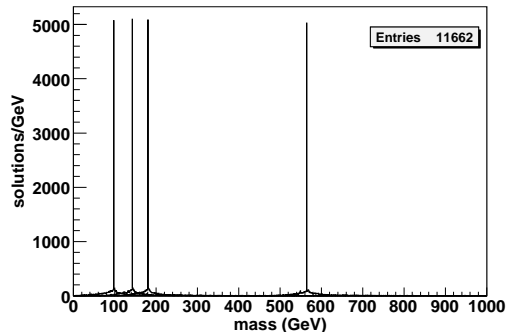


FIG. 2: We plot the number of mass solutions (in 1 GeV bins — the same binning is used for the other plots) vs. mass in the ideal case. All possible pairs for 100 events are included.

For illustration and easy comparison to the literature, we apply our method for the SUSY point, SPS1a [11], although many of the discussions below apply for generic cases. For SPS1a, the particles corresponding to  $N, X, Y, Z$  are  $\tilde{\chi}_1^0, \tilde{\ell}_R(\ell = e/\mu), \tilde{\chi}_2^0, \tilde{q}_L(q = d, u, s, c)$  respectively. The masses are  $\{97.4, 142.5, 180.3, 564.8/570.8\}$  GeV, with the final two numbers corresponding to up/down type squarks respectively. Since  $m_{\tilde{\tau}} \neq m_{\tilde{e}, \tilde{\mu}}$ , the  $\ell = \tau$  case is an important background. We generate events with PYTHIA 6.4 [10].

We first consider the ideal case: no background events, all visible momenta measured exactly, all intermediate particles on-shell and each visible particle associated with the correct decay chain and position in the decay chain. We also restrict the squarks to be up-type only. In this case, we can solve for the masses exactly by pairing any two events. The only complication comes from there being 8 complex solutions for the system of equations, of which more than one can be real and positive. Of course, the wrong solutions are different from pair to pair, but the correct solution is common. The mass distributions for the ideal case with 100 events are shown in Fig. 2. As expected, we observe  $\delta$ -function-like mass peaks on top of small backgrounds coming from wrong solutions. On average, there are about 2 solutions per pair of events.

The  $\delta$ -functions in the mass distributions arise only when exactly correct momenta are input into the equations we solve. To be experimentally realistic, we now include the following.

1. **Wrong combinations.** For a given event a “combination” is a particular assignment of the jets and leptons to the external legs of Fig.1. For each event, there is only one correct combination (excluding  $1357 \leftrightarrow 2468$  symmetry). Assuming that we can identify the two jets that correspond to the two quarks, we have 8 (16) possible combinations for the  $2\mu 2e$  ( $4\mu$  or  $4e$ ) channel. The total number of combinations for a pair of events is the product of the two, *i.e.* 64, 128 or 256. Adding the wrong combination pairings for the ideal case yields the mass distributions of Fig. 3. Compared to Fig. 2, there are

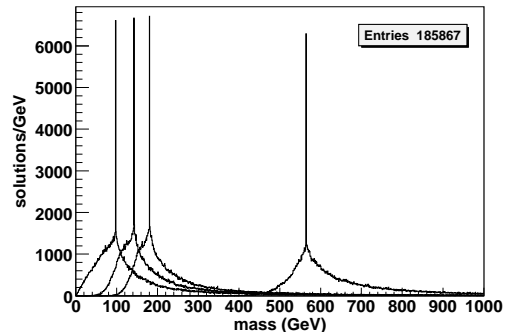


FIG. 3: Number of mass solutions versus mass after including all combination pairings for 100 events.

16 times more (wrong) solutions, but the  $\delta$ -function-like mass peaks remain evident.

2. **Finite widths.** For SPS1a, the widths of the intermediate particles are roughly 5 GeV, 20 MeV and 200 MeV for  $\tilde{q}_L, \tilde{\chi}_2^0$  and  $\tilde{\ell}_R$ . Thus, the widths are quite small in comparison to the corresponding masses.

3. **Mass splitting between flavors.** The masses for up and down type squarks have a small difference of 6 GeV. Since it is impossible to determine flavors for the light jets, the mass determined should be viewed as the average value of the two squarks (weighted by the parton distribution functions).

4. **Initial/final state radiation.** These two types of radiation not only smear the visible particles’ momenta, but also provide a source for extra jets in the events. We will apply a  $p_T$  cut to get rid of soft jets.

5. **Extra hard particles in the signal events.** In SPS1a, many of the squarks come from gluino decay ( $\tilde{g} \rightarrow q\tilde{q}_L$ ), which yields another hard  $q$  in the event. Fortunately, for SPS1a  $m_{\tilde{g}} - m_{\tilde{q}_L} = 40$  GeV is much smaller than  $m_{\tilde{q}_L} - m_{\tilde{\chi}_2^0} = 380$  GeV. Therefore, the  $q$  from squark decay is usually much more energetic than the  $q$  from  $\tilde{g}$  decay. We select the two jets with highest  $p_T$  in each event after cuts. Experimentally one would want to justify this choice by examining the jet multiplicity to ensure that this analysis is dominated by 2-jet events, and not 3 or 4 jet events. Furthermore, the softer jets will be an indication of clearly separable mass-differences.

6. **Background events.** The SM backgrounds are negligible for this signal in SPS1a. There are a few significant backgrounds from other SUSY processes:

(a)  $\tilde{q}_L \rightarrow q\tilde{\chi}_2^0 \rightarrow q\tau\tilde{\tau} \rightarrow q\tau\tau\tilde{\chi}_1^0$  for one or both decay chains, with all  $\tau$ ’s decaying leptonically. Indeed,  $\tilde{\chi}_2^0 \rightarrow \tau\tilde{\tau}$  has the largest partial width, being 14 times that of  $\tilde{\chi}_2^0 \rightarrow \mu\tilde{\mu}$ . However, to be included in our selection the two  $\tau$ ’s in one decay chain must both decay to leptons with the same flavor, which reduces the ratio. A cut on lepton  $p_T$  also helps to reduce this background, since leptons from  $\tau$  decays are softer. Experimentally one should perform a separate search for hadronically decaying tau’s or non-identical-flavor lepton decay chains to

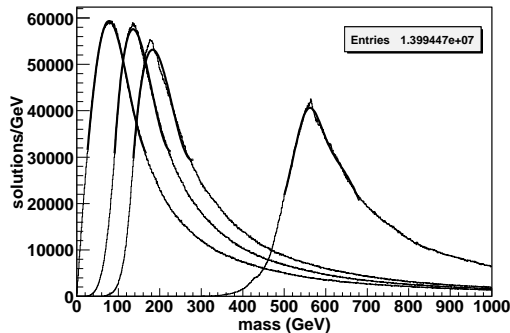


FIG. 4: Mass solutions with all effects 1 – 7 included and after cuts I – III for the SPS1a SUSY model and  $L = 300 \text{ fb}^{-1}$ .

explicitly measure this background.

(b) Processes containing a pair of sbottoms, especially  $\tilde{b}_1$ . In SPS1a the first two generations of squarks are nearly degenerate. In any model, they must be discovered in a combined analysis since light quark jets are not distinguishable. Well-separated squark masses would show up as a double peak structure in  $M_Z$ . However  $b$  jets are distinguishable and a separate analysis should be performed to determine the  $b$  squark masses. This presents a background to the light squark search since  $b$ -tagging efficiency is only about 50% at high  $p_T$ .

(c) Processes that contain a pair of  $\tilde{\chi}_2^0$ 's, not both coming from squark decays. For these events to fake signal events, extra jets need to come from initial and/or final state radiation or other particle decays. For example, direct  $\tilde{\chi}_2^0$  pair production or  $\tilde{\chi}_2^0 + \tilde{g}$  production. These are electroweak processes, but, since  $\tilde{\chi}_2^0$  has a much smaller mass than squarks, the cross-section is not negligible. In our SPS1a analysis, the large jet  $p_T$  cut reduces this kind of background due to the small  $m_{\tilde{g}} - m_{\tilde{q}_L}$ .

**7. Experimental resolutions.** In order to estimate this experimental effect at the LHC, we process all events with ATLFAST[12], a fast simulation package of the ATLAS detector. Since we assume  $300 \text{ fb}^{-1}$  integrated luminosity, we run ATLFAST in the high luminosity mode.

The cuts used to isolate the signal are:

I) 4 isolated leptons with  $p_T > 10 \text{ GeV}$ ,  $|\eta| < 2.5$  and matching flavors and charges consistent with our assumed  $\tilde{\chi}_2^0 \rightarrow \ell \rightarrow \tilde{\chi}_1^0$  decay;

II) No  $b$ -jets and  $\geq 2$  jets with  $p_T > 100 \text{ GeV}$ ,  $|\eta| < 2.5$ . The 2 highest- $p_T$  jets are taken to be particles 7 and 8;

III) Missing  $p_T > 50 \text{ GeV}$ .

For a data sample with  $300 \text{ fb}^{-1}$  integrated luminosity, there are about 1050 events left after the above cuts, out of which about 700 are signal events. After taking all possible pairs for all possible combinations and solving for the masses, we obtain the mass distributions in Fig. 4.

Fitting each distribution using a sum of a Gaussian plus a (single) quadratic polynomial and taking the maximum positions of the fitted peaks as the estimated masses yields  $\{77.8, 135.6, 182.7, 562.0\} \text{ GeV}$ . Averaging over

10 different data samples, we find

$$\begin{aligned} m_N &= 76.7 \pm 1.4 \text{ GeV}, & m_X &= 135.4 \pm 1.5 \text{ GeV}, \\ m_Y &= 182.2 \pm 1.8 \text{ GeV}, & m_Z &= 564.4 \pm 2.5 \text{ GeV}. \end{aligned}$$

The statistical uncertainties are very small, but there exist biases, especially for the two light masses. In practice, we can always correct the biases by comparing real data with Monte Carlo. Nevertheless, we would like to reduce the biases as much as possible using data only. In some cases, the biases can be very large and it is essential to reduce them before comparing with Monte Carlo.

The combinatorial background is an especially important source of bias since it yields peaked mass distributions that are not symmetrically distributed around the true masses, as can be seen from Fig. 3. This will introduce biases that survive even after smearing. Therefore, we concentrate on reducing wrong solutions.

First, we reduce the number of wrong combinations by the following procedure. For each combination choice,  $c$ , for a given event,  $i$  ( $i = 1, N_{evt}$ ), we count the number,  $N_{pair}(c, i)$ , of events that can pair with it (for some combination choice for the 2nd events) and give us solutions. We repeat this for every combination choice for every event. Neglecting effects 2.– 7.,  $N_{pair}(c, i) = N_{evt} - 1$  if  $c$  is the correct combination for event  $i$ . After including backgrounds and smearing,  $N_{pair}(c, i) < N_{evt} - 1$ , but the correct combinations still have statistically larger  $N_{pair}(c, i)$  than the wrong combinations. Therefore, we cut on  $N_{pair}(c, i)$ . For the SPS1a model point, if  $N_{pair}(c, i) \leq 0.75 N_{evt}$  we discard the combination choice,  $c$ , for event  $i$ . If all possible  $c$  choices for event  $i$  fail this criterion, then we discard event  $i$  altogether (implying a smaller  $N_{evt}$  for the next analysis cycle). We then repeat the above procedure for the remaining events until no combinations can be removed. After this, for the example data sample, the number of events is reduced from 1050 (697 signal + 353 background) to 734 (539 signal + 195 background), and the average number of combinations per event changes from 11 to 4.

Second, we increase the significance of the true solution by weighting events by  $1/n$  where  $n$  is the number of solutions for the corresponding pair (using only the combination choices that have survived the previous cuts). This causes each pair (and therefore each event) to have equal weight in our histograms. Without this weighting, a pair with multiple solutions has more weight than a pair with a single solution, even though at most one solution would be correct for each pair.

Finally, we exploit the fact that wrong solutions and backgrounds are much less likely to yield  $M_N, M_X, M_Y$ , and  $M_Z$  values that are all simultaneously close to their true values. We plot the  $1/n$ -weighted number of solutions as a function of the three mass differences (Fig. 5). We define mass difference windows by  $0.6 \times$  peak height and keep only those solutions for which *all three* mass differences fall within the mass difference windows. The

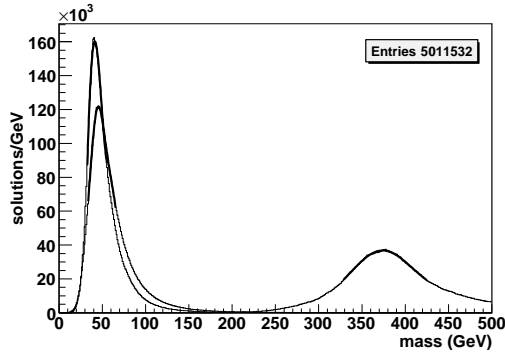


FIG. 5: SPS1a,  $L = 300 \text{ fb}^{-1}$  mass difference distributions.

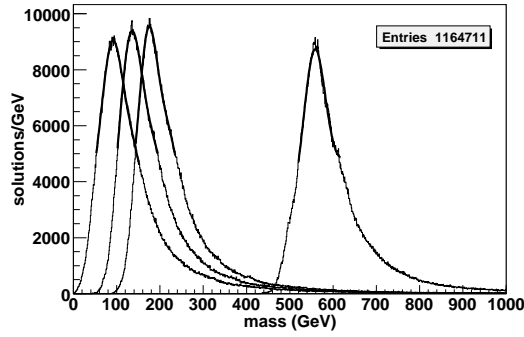


FIG. 6: Final mass distributions after the bias-reduction procedure for the SPS1a SUSY model and  $L = 300 \text{ fb}^{-1}$ .

surviving solutions are plotted (without the  $1/n$  weighting) in Fig. 6. Compared with Fig. 4, the mass peaks are narrower, more symmetric and the fitted values are less biased. The fitted masses are  $\{91.7, 135.9, 175.7, 558.0\}$  GeV. Repeating the procedure for 10 data sets, we find

$$\begin{aligned} m_N &= 94.1 \pm 2.8 \text{ GeV}, & m_X &= 138.8 \pm 2.8 \text{ GeV}, \\ m_Y &= 179.0 \pm 3.0 \text{ GeV}, & m_Z &= 561.5 \pm 4.1 \text{ GeV}. \end{aligned}$$

Thus, the biases are reduced at the cost of (slightly) increased statistical errors.

We have applied our method to other mass points to show its reliability. Details will be presented in [9]. We quote here results for “point 1” defined in Ref. [6] with the following masses:  $\{85.3, 128.4, 246.6, 431.1/438.6\}$  GeV. For  $100 \text{ fb}^{-1}$  data, we have about 1220 events (1160 signal events) after the pre-bias-reduction cuts. After following a bias reduction procedure and using 10 data samples, we obtain  $m_N = 85 \pm 4 \text{ GeV}$ ,  $m_X = 131 \pm 4 \text{ GeV}$ ,  $m_Y = 251 \pm 4 \text{ GeV}$ ,  $m_Z = 444 \pm 5 \text{ GeV}$ .

We emphasize that the remaining biases in the above mass determinations can be removed by finding those input masses that yield the observed output masses after processing Monte Carlo generated data through our procedures. In this way, very accurate central mass values are obtained with the indicated statistical errors.

The above results for the  $N$ ,  $Y$  and  $X$  masses for the SPS1a point and point #1 can be compared to those obtained following a very different procedure in Ref. [6]. There, only the  $X \rightarrow Y \rightarrow N$  parts of the two decay

chains were employed and we used only  $4\mu$  events. For the SPS1a model point we obtained  $m_N = 98 \pm 9 \text{ GeV}$ ,  $m_Y = 187 \pm 10 \text{ GeV}$ , and  $m_X = 151 \pm 10 \text{ GeV}$ . And, for point #1 we found  $m_N = 86.2 \pm 4.3 \text{ GeV}$ ,  $m_X = 130.4 \pm 4.3 \text{ GeV}$  and  $m_Y = 252.2 \pm 4.3 \text{ GeV}$ . Including the  $4e$  and  $2\mu 2e$  channels will reduce these errors by a factor of  $\sim 2$ . The procedure of [6] can thus be used to verify the results for  $m_N$ ,  $m_X$  and  $m_Y$  from the present procedure and possibly the two can be combined to obtain smaller errors than from either one, with  $m_Z$  determined by the procedure of this letter.

Overall, we have obtained a highly-encouraging level of accuracy for the mass determinations in events with two chains terminating in an invisible particle. Once the masses are known with this level of accuracy, the next step will be to examine detailed distributions for various possible models (MSSM, little-Higgs, Universal Extra Dimensions), assuming the determined masses and keeping only solutions for each event consistent with them. The different models can be expected to predict sufficiently distinct distributions (for the same mass choices) that the precise nature of the invisible particle can be determined. We will then be able to make fairly precise predictions for its relic density and check for consistency with observation. Showing that the dark matter particle as observed at the LHC predicts a relic density consistent with cosmological observations would resolve one of the most important issues of modern-day physics.

This work was supported in part by U.S. Department of Energy grant No. DE-FG03-91ER40674.

- 
- [1] B. C. Allanach *et al*, JHEP **0009**, 004 (2000)
  - [2] K. Kawagoe, M. M. Nojiri and G. Polesello, Phys. Rev. D **71**, 035008 (2005)
  - [3] B. K. Gjelsten, D. J. Miller and P. Osland, JHEP **0412**, 003 (2004)
  - [4] D. J. Miller, P. Osland and A. R. Raklev, JHEP **0603**, 034 (2006)
  - [5] In a follow-up study, C. G. Lester discussed a likelihood method using all 5 mass shell constraints, which is in Part X of B. C. Allanach *et al*. [Beyond the Standard Model Working Group], arXiv:hep-ph/0402295.
  - [6] H. C. Cheng, J. F. Gunion, Z. Han, G. Marandella and B. McElrath, JHEP **0712**, 076 (2007)
  - [7] W. S. Cho, K. Choi, Y. G. Kim and C. B. Park, arXiv:0709.0288 [hep-ph].
  - [8] M. M. Nojiri, G. Polesello and D. R. Tovey, arXiv:0712.2718 [hep-ph].
  - [9] H. C. Cheng, D. Engelhardt, J. F. Gunion, Z. Han and B. McElrath, in preparation.
  - [10] T. Sjostrand, S. Mrenna and P. Skands, JHEP **0605**, 026 (2006) [arXiv:hep-ph/0603175].
  - [11] B. C. Allanach *et al.*, in *Proc. of the APS/DPF/DPB Summer Study on the Future of Particle Physics (Snowmass 2001)* ed. N. Graf, Snowmass, Colorado, 30 Jun - 21 Jul 2001, pp P125 [arXiv:hep-ph/0202233].
  - [12] E. Richter-Was, D. Froidevaux, and L. Poggioli, ATLAS-PHYS-98-131; <http://www.hep.ucl.ac.uk/atlas/atlfast/>.